Analysis of high-order sub-harmonically injection-locked oscillators

Silvia Hernández, Mabel Pontón, Sergio Sancho, Almudena Suárez
University of Cantabria, Spain
silvia.hernandez@unican.es

***Abstract* — High-order subharmonically injection-locked oscillators have recently been proposed for low phase-noise frequency generation, with carrier-selection capabilities. This work focuses on the analysis of this frequency-synthesis procedure, with emphasis on the oscillator capability to discriminate the input tones, under the variation of a tuning voltage. The oscillator is described with an analytical envelope-domain formulation, leading to an expression for the oscillator phase shift with respect to the input source. The average of this phase shift is shown to evolve in a continuous manner in the distinct synchronization bands obtained versus the tuning voltage. Then, the subsynchronized operation at a high frequency ratio ($N = 30$) is considered, showing the applicability of envelope-domain simulations under various Fourier decompositions and sampling rates. The synchronization bands are obtained through the phase averaging technique. The analysis has been applied to a prototype at 2.7 GHz that has been manufactured and measured.**

***Keywords* — injection locking, oscillator, envelope transient.**

I. INTRODUCTION

The recent works [1]-[3] present a frequency-synthesis technique based on the subharmonic injection locking of an oscillator at a frequency f_o by an independent source at a much lower frequency. The high ratio N between the two frequencies (in the order of $N = 30$) is enabled by the periodic switching of the higher frequency oscillator by a low frequency input, which gives rise to a high number of spectral lines at the oscillator output. This output signal is introduced into a second oscillator, which gets locked to one or another spectral line, depending on its tuning voltage [1]-[3]. Thus, the combination of the two oscillators enables a programmable frequency selection, with frequency spacing f_o/N. The whole system has the advantage of a low phase noise in comparison with standard phase-locking methodologies [2]. However, the realistic simulation of this complex system is extremely demanding and, to our knowledge, has not been carried out in any previous work. In [1]-[3] the injection-locked oscillator (ILO) is analyzed in time domain, using simplified models of the Van der Pol type. Then, the synchronization bandwidths are detected through a comparison of the oscillation amplitude and phase values at the beginning and end of each period of the switching signal.

Here the analysis will be carried out in the envelope domain [4]-[5], better suited at microwave frequencies. Two distinct investigations will be performed: the oscillator frequency selectivity and its subsynchronized operation under a high frequency ratio. Initially the ILO response in the presence of an arbitrary multitone input signal is analyzed, in terms of bandwidth and spectral content. An analytical formulation is used to derive an expression for the oscillator phase shift with respect to the locking tone. As will be shown, the averaging of this phase shift enables a reliable detection of the distinct synchronization bands obtained versus a tuning parameter. In a second stage, a high subharmonic order ILO is considered. Its envelope-domain analysis is based on a judicious choice of the Fourier frequency basis and integration time step, combined with the phase averaging technique to detect the synchronization bands. The analysis has been applied to a prototype at 2.7 GHz that has been manufactured and measured.

II. FREQUENCY SELECTIVITY

Let an oscillator with an input signal composed of multiple tones, at the frequencies ω_1, $\omega_2,\ldots,\omega_K$, be considered. For a good insight, closely-spaced tones about the free-running frequency, ω_o, will be initially assumed. The oscillator will be modeled in terms of its current-to-voltage ratio $Y(V,\omega,\eta)$ at a particular observation node [6]-[7], where V is the voltage amplitude at ω and η is a tuning parameter. In the absence of the input signals, one has $Y(V_o, \omega_o, \eta_o) = 0$, where V_o and ω_o, are the free-running amplitude and frequency at η_o. The oscillator will be formulated at the particular input frequency ω_q, expressing the node voltage as $(V_o+\Delta V(t))e^{j\phi(t)}e^{j\omega_q t}$. Applying the implicit function theorem [6]-[7] to the circuit-level envelope-transient system, one obtains the following equation:

$$Y\left(V_o+\Delta V(t),\eta_o+\Delta\eta,\omega_o+\Delta\omega_q+s/j\right)\left(V_o+\Delta V(t)\right)e^{j\phi(t)}= =\sum_k \frac{I_k}{V_o}\exp j\left(\Delta\omega_{k,q}t\right),\quad \Delta\omega_{k,q}=\omega_k-\omega_q \tag{1}$$

where s is a complex frequency increment and I_k is the complex equivalent current of the each input signal. Under small input power and close spacing of the input tones, the function Y can be expressed in a first-order Taylor series expansion about V_o, ω_o and η_o [6]-[7]. Taking into account that s acts as a time differentiator, one obtains:

$$Y_V\Delta V(t)+Y_\eta\Delta\eta+Y_\omega\left(\Delta\omega_q+\dot{\phi}(t)-j\Delta\dot{V}(t)/V_o\right)= =\sum_k \frac{I_k}{V_o}\exp j\left(-\phi(t)+\Delta\omega_{k,q}t\right) \tag{2}$$

where $\Delta\omega_q=\omega_q-\omega_o$ and Y_V, Y_η and Y_ω are the derivatives of Y with respect to V, η and ω, calculated at V_o, ω_o, η_o, as shown in [6]-[7]. Solving for $\Delta\omega_q+\dot{\phi}(t)$:

$$\Delta\omega_q + \dot{\phi}(t) = \frac{-|Y_\eta| \sin\alpha_{v\eta}\Delta\eta + \sum_k \frac{|I_k|}{V_o}\sin\left(-\phi(t) + \Delta\omega_{k,q}t + \phi_k - \alpha_v\right)}{|Y_\omega|\sin\alpha_{v\omega}} \quad (3)$$

where $|I_k|$ and ϕ_k are the magnitude and phase of the input tones, $\alpha_{v\omega} = ang(Y_\omega)$-$ang(Y_V)$, $\alpha_{v\eta} = ang(Y_\eta)$- $ang(Y_V)$ and $\alpha_v = ang(Y_V)$. The phase $\phi(t)$ can be expressed as $\phi(t) = \phi_o + \Phi_{mix}(t)$, where ϕ_o is a constant value. Under synchronization at ω_q, the phase $\phi(t)$ in (3) can be represented in a Fourier series at K-1 frequencies $\Delta\omega_{1,q},...,\Delta\omega_{K,q}$, so $\Phi_{mix}(t)$ has zero average. Averaging equation (3):

$$\Delta\omega_q = \frac{|I_q|}{V_o}\frac{\sin(-\phi_o - \alpha_v)}{|Y_\omega|\sin\alpha_{v\omega}} - \frac{|Y_\eta|\sin\alpha_{v\eta}}{|Y_\omega|\sin\alpha_{v\omega}}\Delta\eta + \frac{\left\langle \sum_k \frac{|I_k|}{V_o}\sin\left(-\Phi_{mix}(t) + \Delta\omega_{k,q}t + \phi_k - \alpha_v\right)\right\rangle}{|Y_\omega|\sin\alpha_{v\omega}} \quad (4)$$

From inspection of (4), $\Delta\eta$ depends on ϕ_o, which varies between 0 to 2π, and the averaged term on the right side. As in the case of an oscillator locked to a single tone, only about one half of the total phase ϕ_o range (from 0 to 2π) will correspond to stable solutions. As derived from (2), the voltage magnitude at ω_q is V_o+$\Delta V(t)$, so the power at ω_q is enhanced by the self-oscillation. The increment $\Delta V(t)$ is:

$$\Delta V(t) = \frac{\frac{|I_q|}{V_o}\sin(\alpha_\omega + \phi_o)}{|Y_V|\sin\alpha_{v\omega}} - \frac{|Y_\eta|\sin\alpha_{\eta\omega}}{|Y_V|\sin\alpha_{v\omega}}\Delta\eta + \frac{\sum_k \frac{|I_k|}{V_o}\sin\left(\alpha_\omega + \Phi_{mix}(t) + \phi_k - \Delta\omega_{k,q}t\right)}{|Y_V|\sin\alpha_{v\omega}} \quad (5)$$

where $\alpha_\omega = ang(Y_\omega)$, $\alpha_{\eta\omega} = ang(Y_\omega)$-$ang(Y_\eta)$. The first two terms in (5) are not frequency dependent and the first one increases with the magnitude $|I_q|$.

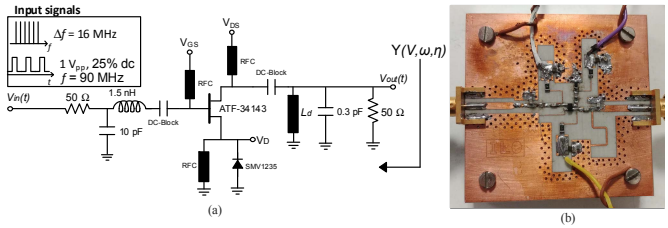

Fig. 1. FET-based (ATF-34143) oscillator at f_o = 2.7 GHz. The frequency is tuned with the varactor diode SMV1235. (a) Schematic. (b) Photograph.

The above analysis has been applied to the voltage-controlled oscillator at f_o = 2.7 GHz in Fig. 1, tuned with the varactor SMV1235. The tones, generated with the Agilent E4438C ESG Vector Signal Generator, are equally spaced by default. In order to generate as many tones as possible, the spacing Δf = 16 MHz is chosen, enabling six input tones, between 2.7 GHz and 2.78 GHz. Initially, synchronization at $\omega_q/(2\pi)$ = 2.7 GHz is assumed. Fig. 2 validates the spectrum obtained through the integration of (2) and with circuit-level envelope transient simulations [4]-[5], using ω_q as the only fundamental frequency, as in (2). Fig. 3(a) presents the phase shift $-\phi(t)$ for three different values of $\eta = V_D$, within the synchronization band. In agreement with (3), after a transient, the phase exhibits a periodic variation about a constant value (-ϕ_o), which changes with V_D. To obtain the synchronization bandwidth, the average value of $-\phi(t)$ is represented versus V_D [Fig. 3(b)]. This requires a sufficiently large time offset to ensure that the circuit is in steady state at each V_D step. The apparent discontinuities in the diagram are because the fundamental frequency of the envelope-domain analysis, ω_q, is alternatively set to each of the input frequencies. Otherwise there will be an additional ramp function $(\omega_q - \omega_k)t$ in $\Phi_{mix}(t)$. The synchronization bands are easily distinguished (in solid line), since $\langle -\phi(t)\rangle = -\phi_o$ varies continuously in each band, with an excursion of slightly less than 180º, corresponding to the stable solutions. This excursion is not centered about ϕ_o = 0º because α_v is different from zero. The three bands in Fig. 3(b) correspond to synchronization at f_1 = 2.7 GHz, f_2 = 2.716 GHz and f_3 = 2.732 GHz.

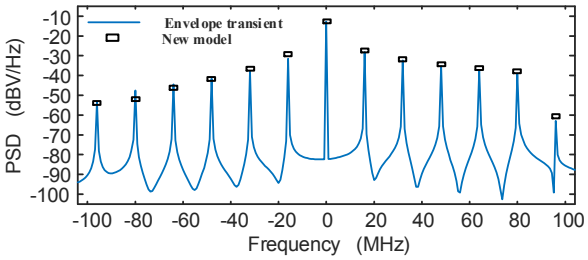

Fig. 2. Spectrum obtained through (2) and with envelope transient for the spectral-line power P_{in} = –33 dBm and frequency spacing Δf = 16 MHz.

The frequency selection capabilities are evaluated without changing the frequency basis, kept at ω_q. The frequencies of the three dominant spectral lines (those having the largest output power values) are identified and traced versus V_D [Fig. 3(c)]. The circuit is synchronized where the frequencies are constant. In Fig. 3(d) the output power at the frequencies of the input tones is evaluated versus V_D. The boundaries of the synchronization bands are easily detected by the discontinuity of the curves. The bandwidths slowly decrease when moving away from the oscillator free-running frequency (2.7 GHz). Fig. 4 presents the measurement results. Fig. 4(a) shows the six input tones, with Δf = 16 MHz. Fig. 4(b) presents an unlocked spectrum for V_D = 0.28 V. Fig. 4(c) and (d) present the spectrum for V_D = 0.8 V (synchronization to f_2), and V_D = 2.85 V (to f_5). There is a deviation in the tuning voltages, attributed to the inaccuracies in the device models.

III. Sub-harmonic Injection Locked Operation

The analysis of the subharmonically synchronized oscillator is more demanding than the one in Section II, since the subsynchronization is a nonlinear phenomenon and the relevant spectral lines, resulting from the input signal, plus frequency multiplication/mixing effects, cover the entire frequency bandwidth from dc to the oscillation frequency (and all the frequency intervals between the harmonic terms). The harmonic balance (HB) analysis of a subsynchronized solution at a high order, such as N = 30 considered here, is

computationally very costly. For instance, to account for 3 harmonic components of the oscillation frequency f_o, the number NH of harmonic terms must be $NH = 3N = 90$. On the other hand, the envelope-transient analysis demands some considerations. When expressing the state variables in a Fourier basis at the fundamental frequency f_o, the system integration requires a small time step Δt, able to capture the large bandwidth going from dc to approximately $f_o/2$. As a compromise, one can use a basis having f_o/P as fundamental frequency, where the integer P fulfils $P<N$. Assuming, for better insight, a reduced-order formulation from a single observation node, the outer-tier envelope-transient system is:

$$
\begin{aligned}
&G\left(V_0(t),\tilde{V}_1(t),\ldots,\tilde{V}_P(t),s/j\right)V_o(t)=\sum_{k=1}^{B/2}\frac{I_k}{V_o}\exp j\left(\omega_k t\right),\\
&Y_1\left(V_0(t),\tilde{V}_1(t),\ldots,\tilde{V}_P(t),\omega_o/P+s/j\right)\tilde{V}_1(t)=\\
&\sum_{k=1+B/2}^{B+B/2}\frac{I_k}{V_o}\exp j\left(\Delta\omega_{1,k}t\right),\ \ \Delta\omega_{1,k}=\omega_k-\omega_o/P\\
&\vdots\\
&Y_p\left(V_0(t),\tilde{V}_1(t),\ldots,\tilde{V}_P(t),p\omega_o/P+s/j\right)\tilde{V}_p(t)=\\
&\sum_{k=1+(p-1)B+B/2}^{1+pB+B/2}\frac{I_k}{V_o}\exp j\left(\Delta\omega_{p,k}t\right),\ \Delta\omega_{p,k}=\omega_k-p\omega_o/P\\
&\vdots\\
&Y_P\left(V_0(t),\tilde{V}_1(t),\ldots,\tilde{V}_P(t),\omega_o+s/j\right)\tilde{V}_P(t)=\\
&\sum_{k=1+(P-1)B+B/2}^{M}\frac{I_k}{V_o}\exp j\left(\Delta\omega_{P,k}t\right),\ \Delta\omega_{P,k}=\omega_k-\omega_o
\end{aligned}
\qquad (6)
$$

where $\tilde{V}_p(t)$ indicates phasors. In (6), the integer $B/2$ is the number of spectral lines at each side of the p-th subharmonic component, pf_o/P, where $p=1,\ldots,P$. Thus, the total number of spectral lines is given by $M=B/2+PB$. The frequency-domain models of the distributed components must be valid in the whole bandwidth of each harmonic component. For a higher P, the integration time step can, in principle, be increased as $P\Delta t$. Note that the equation at each harmonic p is analogous to the one in (1). The phasors $\tilde{V}_p(t)$, with the phases $\phi_p(t)=\phi_{o,p}+\Phi_{mix,p}(t)$, will exhibit a slower time variation for a higher P. In the limit situation $P=N$, the phasors $\tilde{V}_p$ will be constant in the synchronization band.

The oscillator in Fig. 1 has been injection-locked by a rectangular signal with frequency 90 MHz, amplitude 1 Vpp, and duty-cycle of 25%. To facilitate the locking, the input dc block has been suppressed. Although the oscillation frequency of this prototype (2.7 GHz) is lower than the one in [1]-[3], the frequency ratio is the same $N=30$, so the analysis complexity must be similar. The circuit has been analysed with circuit-level envelope transient, following the criteria in (6), and using an auxiliary generator (AG) at f_o, connected to the circuit at the initial time only [6], to initialize the oscillation. Fig. 5(a) presents the spectrum at $f_{out}=30\times90$ MHz for $P=1,4,6$, which predicts a synchronized behaviour. Only the central spectral lines can agree since for $P>1$ part of the spectrum corresponds to terms P-1 and P+1. For $P=1$ the integration time step is 0.05 ns, whereas for $P=6$ it is 0.3 ns. With P = 6, the time variation is more regular and the synchronization bands can be determined with higher accuracy. The analysis has been validated through an independent HB analysis (superimposed). This costly HB analysis has been carried out providing the amplitude and phase of the central spectral line, obtained with envelope transient, to an AG at $f_{out}=30\times90$ MHz.

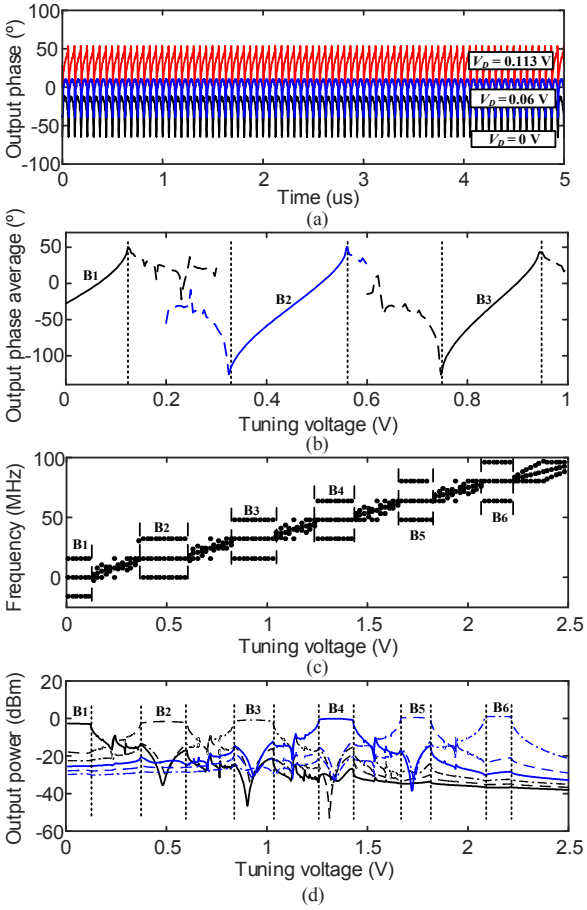

Fig. 3. Behavior under six input lines, between 2.7 GHz and 2.78 GHz, with Δf = 16 MHz. (a) Time variation of the phase shift for three V_D values, within the first synchronization band (f_1 = 2.7 GHz). (b) Average value of $-\phi(t)$ versus V_D. (c) Frequencies of the three spectral lines with larger output power, traced versus V_D. (d) Output power at the frequencies of the input tones.

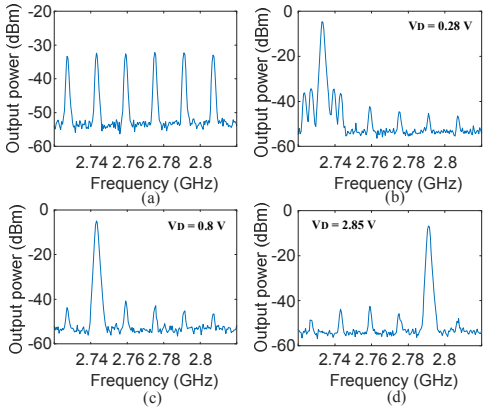

Fig. 4. Measurement results. (a) Input tones. (b) Unlocked spectrum for V_D = 0.28 V. (d) Synchronization to f_2 for V_D = 1.69 V. (e) f_4 for V_D = 2.85 V.

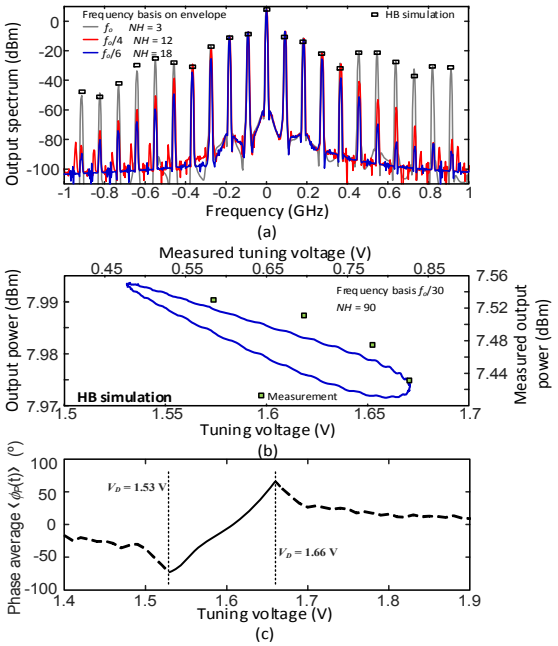

Fig. 5 Injection locking by a pulsed signal at 90 MHz. (a) Output spectrum at $f_{out} = 30\times 90$ MHz when considering P = 1,4,6. HB results are superimposed. (b) Synchronization curve, versus V_D, obtained with HB. Experimental points are superimposed. (c) Synchronization band obtained through the calculation of $\langle\phi_P(t)\rangle = \phi_{o,P}$, with the method in Section II.

Through AG optimization [7], it was possible to trace the synchronization curve versus V_D [Fig. 5(b)] using HB, which took approximately 3 hours. Experimental points are superimposed. Fig. 5(c) presents the analysis of the synchronization band with the phase averaging method proposed in Section II, which is computationally more efficient. The analysis is based on the averaging of the phase of the P-th harmonic component of the output voltage, that is, on the calculation of $\langle\phi_P(t)\rangle = \phi_{o,P}$, which has been traced versus V_D. Note that envelope transient only provides the upper (stable) section of the synchronization curve. There is an excellent agreement with the HB predictions, though the computation time is four times shorter. Moreover, it was not possible to obtain any HB convergence when changing V_D in order to select a different spectral line, for instance N+1 and N+2. This could be easily done with the envelope-transient method, as shown in Fig. 6(a), where three different spectral lines, corresponding to N = 30, N+1 and N+2, are selected by changing V_D. Finally, the output of the subsynchronized oscillator has been connected to an analogous voltage-controlled oscillator to increase the frequency selectivity. To initialize the two individual oscillations an AG is connected to each circuit at the initial time only. The simulated spectra are shown in Fig. 6(b). The ratio between the selected spectral line and the highest-power neighbouring line is in the order of 30 dB. Fig. 6(c) presents the experimental results. In a manner similar to Fig. 4, there is a deviation in the tuning voltages, attributed to the device models.

IV. Conclusion

An envelope-domain analysis of high-order subharmonically injection-locked oscillators has been presented. The locking bands can be efficiently detected by averaging the phase of the oscillation spectral line. Application of this technique to a high-order subharmonic synchronization requires a suitable selection of the Fourier decomposition and time sampling. The procedure has been illustrated with a two-oscillator system at the subharmonic order N = 30. To our knowledge, it is the first realistic analysis of a system of this high complexity.

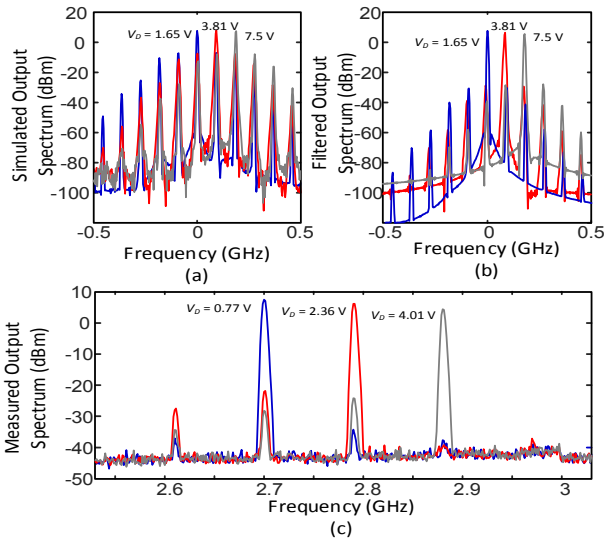

Fig. 6. Carrier-frequency selection. (a) Spectra when varying V_D to select f_1 = 2.7 GHz (N= 30), f_2 = 2.79 GHz (N+1) and f_3 = 2.88 GHz (N+2). (b) Same analysis in the presence of a second oscillator, used to increase the frequency selectivity. (c) Measured spectra of the two-oscillator system.

Acknowledgment

This work was supported by the Spanish Ministry of Science, Innovation and Universities and the European Regional Development Fund (ERDF/FEDER) under the research project TEC2017-88242-C3-1-R.

References

[1] C. Jany, A. Siligaris, P. Ferrari and P. Vincent, "A novel programmable harmonic selection technique based on the pseudo-locking of an oscillator by periodically repeated oscillations train," *44th European Microwave Conference (EuMC)*, Rome, Italy, 2014, pp. 1020-1023.

[2] C. Jany, A. Siligaris, J. L. Gonzalez-Jimenez, P. Vincent and P. Ferrari, "A Programmable Frequency Multiplier-by-29 Architecture for Millimeter Wave Applications," *IEEE J. Solid-State Circuits*, vol. 50, no. 7, pp. 1669-1679, Jul., 2015.

[3] C. Jany, A. Siligaris, P. Ferrari and P. Vincent, "A novel harmonic selection technique based on the injection of a periodically repeated oscillations train into an oscillator," *IEEE MTT-S Int. Microw. Symp. (IMS2014)*, Tampa, FL, 2014, pp. 1-3.

[4] E. Ngoya and R. Larcheveque, "Envelop transient analysis: a new method for the transient and steady state analysis of microwave communication circuits and systems," *IEEE MTT-S Int. Microwave Symp. Dig.*, San Francisco, CA, USA, 1996, vol.3, pp. 1365-1368.

[5] K. S. Kundert, "Introduction to RF simulation and its application," *IEEE J. Solid-State Circuits*, vol. 34, no. 9, pp. 1298-1319, Sep 1999.

[6] S. Sancho, M. Ponton and A. Suarez, "Effects of Noisy and Modulated Interferers on the Free-Running Oscillator Spectrum," *IEEE Trans. Microw. Theory Techn.*, vol. 66, no. 4, pp. 1831-1842, April 2018.

[7] F. Ramírez, S. Sancho, M. Pontón and A. Suárez, "Analysis of Chirped Oscillators Under Injection Signals," *IEEE MTT-S Int. Microw. Symp - IMS*, Philadelphia, PA, 2018, pp. 172-175.